AIAA JOURNAL
Vol. 40, No. 7, July 2002

Large-Eddy Simulation of a Turbulent Compressible Round Jet

James R. DeBonis*
NASA John H. Glenn Research Center at Lewis Field, Cleveland, Ohio 44135
and
James N. Scott†
The Ohio State University, Columbus, Ohio 43210

A large-eddy simulation (LES) of a high-Reynolds-number jet was performed. A numerical scheme that is uniformly fourth-order accurate in time and space was used to solve the Favre-filtered Navier–Stokes equations. The subgrid-scale stresses were computed using a compressible form of Smagorinsky's model. A cold Mach 1.4 nozzle with a Reynolds number of 1.2×10^6 was simulated. In contrast to similar studies, the entire nozzle geometry including the nozzle lip was modeled. The LES simulation accurately captures the physics of the turbulent flow. The agreement with experimental data is relatively good and improves on results in the current literature. This improvement can be attributed to the numerical scheme and the modeling of the nozzle. In addition, a two-point correlation technique was used to quantify the turbulent structures in the jet mixing layer and showed that computational techniques can be used to characterize such structures for application to Lighthill's acoustic analogy. Two-point space correlations were used to obtain a measure of the integral length scale, which proved to be approximately $\frac{1}{2}D_j$. Two-point space-time correlations were used to estimate the convection velocity for the turbulent structures. This velocity estimates ranged from 0.57 to 0.71 U_j and is in agreement with theory.

Nomenclature

C	=	Smagorinsky model coefficient
C_I	=	Smagorinsky model coefficient
C_ϵ	=	subgrid-scale turbulent dissipation rate model coefficient
c_p	=	specific heat at constant pressure
D_j	=	jet diameter
e_t	=	total energy per unit mass
$\mathcal{L}$	=	length of jet potential core
ℓ	=	integral length scale
Pr	=	Prandtl number
Pr_t	=	turbulent Prandtl number
p	=	pressure
Q_i	=	subgrid-scale heat-flux vector
$\mathcal{R}$	=	correlation coefficient
Re_j	=	Reynolds number based on jet diameter
S_{ij}	=	strain rate tensor
T	=	temperature
t	=	time
U	=	velocity
U_c	=	convective velocity
U_θ	=	velocity at angle θ to the jet axis
u, v, w	=	velocity components
u_i	=	velocity vector
x, y, z	=	Cartesian coordinates
x_i	=	coordinate vector
γ	=	ratio of specific heats
Δ	=	filter width
δ_{ij}	=	Kronecker delta
ϵ	=	turbulent dissipation rate
μ	=	dynamic viscosity
ρ	=	density
σ_{ij}	=	stress tensor
τ	=	time delay for two-point correlation
τ_{ij}	=	subgrid-scale stress tensor
ϕ_i	=	two-point correlation position vector
ψ_i	=	two-point correlation separation vector

Subscripts

exp	=	experiment
j	=	jet
LES	=	large-eddy simulation
0	=	stagnation/total condition
∞	=	freestream

Superscripts

$\bar{}$	=	spatially filtered quantity
$\tilde{}$	=	Favre-filtered quantity
$\hat{}$	=	resolved quantity
$=$	=	time-averaged quantity
$'$	=	unresolved quantity
$''$	=	perturbation from time-averaged value
$\hat{}$	=	turbulent intensity

Received 12 April 2001; revision received 25 January 2002; accepted for publication 5 March 2002.

*Aerospace Engineer, Nozzle Branch. Senior Member AIAA.
†Associate Professor, Department of Aerospace Engineering and Aviation. Associate Fellow AIAA.

Introduction

IN the commercial aircraft industry reducing the noise generated by the aircraft has become an important focus, as communities have begun to impose increasingly stringent restrictions on noise levels near airports. The primary contribution to community noise is jet noise from the engine at takeoff. The behavior of turbulent jets and the mechanisms by which they generate sound are not well understood. Expanding the bounds of knowledge in jet aeroacoustics has become the focus of several recent national programs including NASA's High Speed Research and Advanced Subsonic Technology programs.

Computational fluid dynamics (CFD) has the potential to significantly increase the understanding of jet flows. CFD methods can provide detailed data for the entire jet flowfield. However, current methods using Reynolds-averaged Navier–Stokes (RANS) techniques, which model all of the turbulent scales in the flow, provide only a time average of the flowfield. Large-eddy simulations (LES) offer the potential for a more realistic representation of the flow physics, and hence, improved predictions. LES methods directly compute the large-scale turbulent structures that carry the majority

Table 1 Nozzle and ambient conditions

Quantity	Symbol	Value
Ratio of specific heats	γ	1.4
Nozzle plenum pressure	p_{0_j}	312,410.0 Pa
Nozzle plenum temperature	T_{0_j}	300.0 K
Nozzle exit Mach number	M_j	1.395
Nozzle exit diameter	D_j	0.0254 m
Jet velocity	U_j	411.0 m/s
Ambient pressure	p_∞	98,862.0 Pa
Ambient temperature	T_∞	297.0 K
Reynolds number	Re_j	1.2×10^6

of the energy and model only the small-scale turbulence. As a result, LES provides unsteady/turbulent flowfield data that can be used to determine the turbulent and acoustic characteristics of the jet.

A large-eddy simulation of a turbulent compressible jet from a nearly perfectly expanded axisymmetric nozzle was performed. The jet has a Reynolds number of 1.2×10^6 and an exit Mach number of 1.4. The nozzle exhausted into quiescent air. Table 1 summarizes the nozzle and ambient conditions.

A complete description of the jet flowfield is presented. The time-averaged flowfield is compared to the experimental data of Panda and coworkers[1–3] to assess the accuracy of the simulation. Instantaneous flowfield data and turbulent statistics lend insight into the complex behavior of the jet. Correlation of the velocity signals in the jet's mixing layer help quantify the characteristics of the large-scale structures.

Governing Equations

The Favre-filtered Navier–Stokes equations were solved, and the subgrid-scale turbulent stresses were modeled. The subgrid-scale modeling is based on the incompressible Smagorinsky model.[4] Additional terms to account for compressibility were added based on the work of Moin et al.[5] and Vreman et al.[6]

The continuity equation is

$$\frac{\partial \bar{\rho}}{\partial t} + \frac{\partial \bar{\rho}\tilde{u}_i}{\partial x_i} = 0 \tag{1}$$

The momentum equation is

$$\frac{\partial \bar{\rho}\tilde{u}_i}{\partial t} + \frac{\partial \bar{\rho}\tilde{u}_i\tilde{u}_j}{\partial x_j} + \frac{\partial \bar{p}}{\partial x_i} = \frac{\partial}{\partial x_j}(\hat{\sigma}_{ij} - \tau_{ij}) \tag{2}$$

where the resolved stress tensor is

$$\hat{\sigma}_{ij} = 2\tilde{\mu}\tilde{S}_{ij} - \tfrac{2}{3}\tilde{\mu}\delta_{ij}\tilde{S}_{kk} \tag{3}$$

the Favre-filtered strain rate tensor is

$$\tilde{S}_{ij} = \frac{1}{2}\left(\frac{\partial \tilde{u}_j}{\partial x_i} + \frac{\partial \tilde{u}_i}{\partial x_j}\right) \tag{4}$$

and the subgrid-scale stress tensor is modeled as

$$\tau_{ij} = -2C\bar{\rho}\Delta^2|\tilde{S}|\left(\tilde{S}_{ij} - \tfrac{1}{3}\tilde{S}_{kk}\delta_{ij}\right) + \tfrac{2}{3}C_I\bar{\rho}\Delta^2|\tilde{S}|^2\delta_{ij} \tag{5}$$

The energy equation is

$$\frac{\partial \bar{\rho}\tilde{e}_t}{\partial t} + \frac{\partial \bar{\rho}\tilde{u}_i\tilde{e}_t}{\partial x_i} + \frac{\partial \tilde{u}_i\bar{p}}{\partial x_i} = \frac{\partial \tilde{u}_i\hat{\sigma}_{ij}}{\partial x_i} - \frac{\partial}{\partial x_i}(\hat{q}_i - Q_i) + \epsilon \tag{6}$$

where the total energy is

$$e_t = e + \tfrac{1}{2}\tilde{u}_k\tilde{u}_k + \frac{\tau_{kk}}{2\bar{\rho}} \tag{7}$$

the resolved heat flux is

$$\hat{q}_i = -\tilde{\mu}\frac{c_p}{Pr}\frac{\partial \tilde{T}}{\partial x_i} \tag{8}$$

and the subgrid-scale heat flux is modeled as

$$Q_i = -C\bar{\rho}\Delta^2|\tilde{S}|\frac{c_p}{Pr_t}\frac{\partial \tilde{T}}{\partial x_i} \tag{9}$$

A model for the subgrid-scale turbulent dissipation rate was proposed by Vreman et al.[6] and was used here:

$$\epsilon = \frac{C_\epsilon\bar{\rho}}{\Delta}\left(\frac{\tau_{kk}}{2\bar{\rho}}\right)^{\frac{3}{2}} \tag{10}$$

Sutherland's law was used to compute dynamic viscosity.

The filter width Δ was chosen to be a characteristic length of the computational grid. Because the grid is not uniform, this length varies widely over the grid. The filter width at each location was defined as the cubed root of the volume associated with each grid point:

$$\Delta = (\Delta_x\Delta_y\Delta_z)^{\frac{1}{3}} \tag{11}$$

The constants for the subgrid-models were chosen based on previous studies. Erlebacher et al.,[7] Moin et al.,[5] and Vreman et al.[6] derived the model constants based on direct numerical simulation results. Erlebacher concluded that $C = 0.012$, and Moin gave a range of values of $0.008 \le C \le 0.014$. Moin also provide a range of values for C_I, where $0.0025 \le C_I \le 0.009$. From these data the coefficients were chosen to be $C = 0.012$ and $C_I = 0.00575$. Vreman determined that $C_\epsilon = 0.6$.

Numerical Method

Numerical Scheme

The equations are solved in generalized curvilinear coordinates using a uniformly fourth-order-accurate numerical scheme.[8,9] This scheme combines a five-stage fourth-order low-dispersion Runge–Kutta time-stepping algorithm[10] with a fourth-order central difference spatial operator. Artificial dissipation is provided, for stability, through a solution filtering technique. The sixth-order filter of Kennedy and Carpenter[11] was chosen and provides adequate damping of spurious waves without adversely affecting the truncation error of the scheme. The resulting analysis code was run in parallel on a shared memory Silicon Graphics PowerChallenge workstation.

Computational Grid

The grid accurately models both the external jet flowfield and the nozzle geometry, including the nozzle lip. Previous studies have started their calculations at the nozzle exit plane with an assumed inflow jet velocity profile. This neglects radial variation in the velocity profile caused by the internal nozzle expansion, effects of under- or overexpansion of the nozzle flow, and the effect of the nozzle lip geometry on the stability and growth rate of the mixing layer.

The initial computational grid used in the study is pictured in Fig. 1. The dimensions of the grid were chosen based on a grid density study performed using an axisymmetric analysis.[8] The resulting axisymmetric grid contains 301 points in the streamwise direction and 129 points in the radial direction. The resolution in the azimuthal direction was set by placing one grid plane at every 10 deg. Four additional planes were necessary to overlap the grid onto itself in order to maintain fourth-order accuracy at the boundary. The computational domain extends 20 jet diameters downstream of the nozzle exit and 10 jet diameters from the jet centerline. This "coarse" grid has dimensions $301 \times 129 \times 40$ and contains 1.5 million grid points. For this grid the spacing in the azimuthal direction is much larger than the corresponding spacing in the axial and radial directions. A second grid with greater resolution in the azimuthal direction was created. To keep the computational cost down, the length of the domain in the streamwise direction was reduced from $20D_j$ to $15D_j$. The azimuthal resolution was increased by placing one grid plane at every 6 deg (64 planes, including the 4 plane overlap). This "fine" grid has dimensions $280 \times 129 \times 64$ and contains 2.3 million grid points.

Boundary Conditions

Boundary conditions based on the local one-dimensional propagation of flow properties were used at the inflow and outflow. While the jet exited into quiescent air in the experiment, a Mach 0.05 freestream was used in the calculation to maintain well-posed boundaries conditions. This approximation was shown to have very

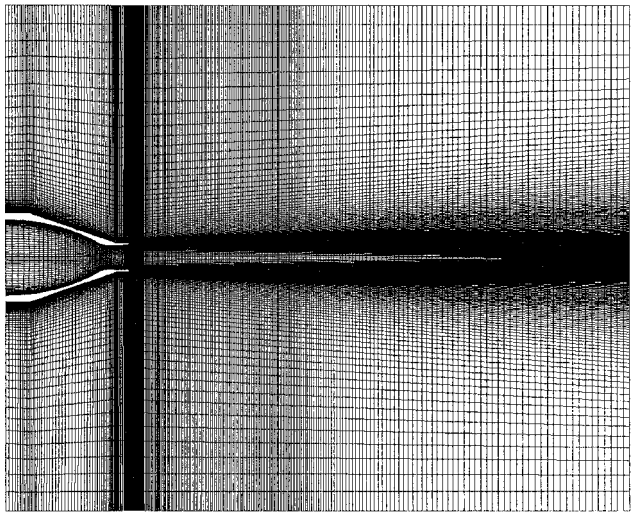

Streamwise, x–y plane

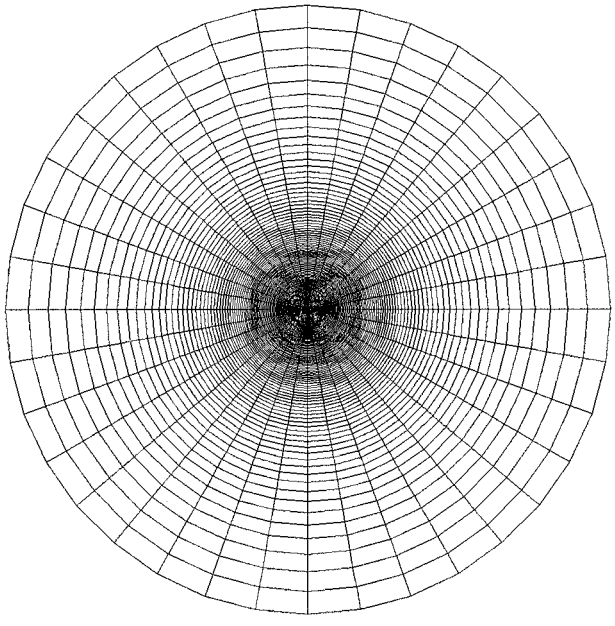

Cross-stream, y–z plane at outflow boundary

Fig. 1 Computational grid.

little effect on the flowfield for RANS calculations of jet flows.[12] Total pressure and temperature were specified in the nozzle plenum. The use of an exit zone to damp reflected waves from the outflow boundary was explored in a previous study[8] and found not to be necessary for this case. The grid spacing at the upper and downstream limits of the domain are sufficiently large that the numerical scheme damps any reflected waves without any additional treatment. A subsonic outflow boundary condition, which imposes a static pressure, was specified on the outer portion of the boundary. Near the jet centerline all conditions were extrapolated to allow for structures with supersonic velocity to exit the domain properly. A far-field characteristic condition was specified on the outer boundary. The conditions on the singularity along the jet axis were obtained by averaging the conditions around the singularity. The no-slip condition was imposed on the nozzle surfaces. The relatively large grid spacing at the nozzle wall precludes capturing any turbulent structures in the boundary layer. There was also no additional modeling, such as a RANS turbulence model, to simulate a turbulent boundary layer. As a result, the simulation produces a laminar boundary on the nozzle walls. This is a reasonable approximation of the experiment where only very small density fluctuations were measured in this region.[3]

Results

The LES simulation was started from uniform initial freestream conditions, and the jet was impulsively started. Three-dimensional turbulent structures developed naturally without any external perturbation. As already stated, a sixth-order solution filter was used. Both 10th- and 8th-order filters were tried, but they failed to provide adequate stability around the shock structures found at the nozzle exit. Once the flowfield was established, it was run approximately two acoustic times (the time required for a sound wave to traverse the domain) before data were saved for analysis. The code was then run an additional two acoustic times to obtain data. Before stopping the analysis, the time-averaged centerline velocity profile was checked to ensure that it remained unchanged for over 5000 iterations. It was observed that in the region of the jet downstream of the potential core $x/D_j > 8$ the flow structures were of a much lower frequency than in the upstream portions of the jet, resulting in poorer averaging in this area. This observation was also made by Boluriaan et al.[13] As shown later, in the primary area of interest $x/D_j < 8$, the flowfield averages and resulting turbulent correlations are well converged. Using 16 processors on a Silicon Graphics Power Challenge machine, the simulation required about two months of calendar time for completion. Data were sampled every 100 iterations for analysis.

Contours comparing instantaneous and time-averaged velocities in both the streamwise and cross-stream planes are presented in Figs. 2–7. The difference between the instantaneous and time average is clear and illustrates the additional information provided by an unsteady calculation. The instantaneous velocities show large turbulent structures that cannot be discerned from the mean flow. Large azimuthal velocities and the appearance of turbulent structures that cross the jet axis near the end of the potential core indicate a highly three- dimensional flowfield.

The time-averaged velocities closely resemble both experimental data and RANS calculations. But, clearly the LES solution is capable of providing much more insight into the flow physics of the jet through the unsteady information.

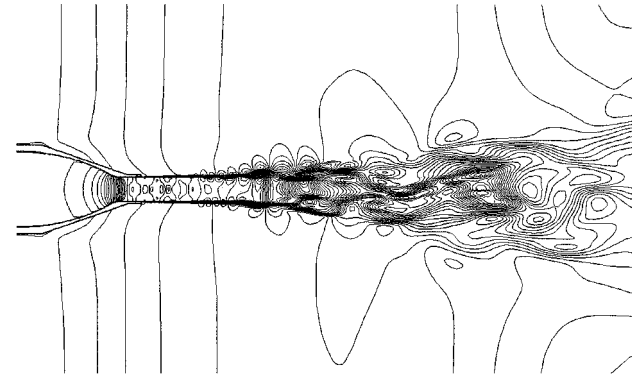

Instantaneous

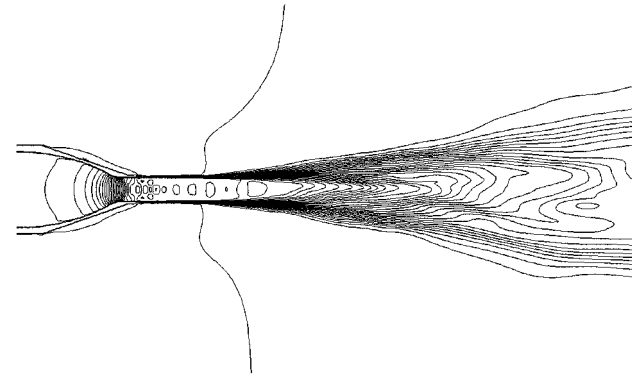

Time averaged

Fig. 2 Axial velocity contours.

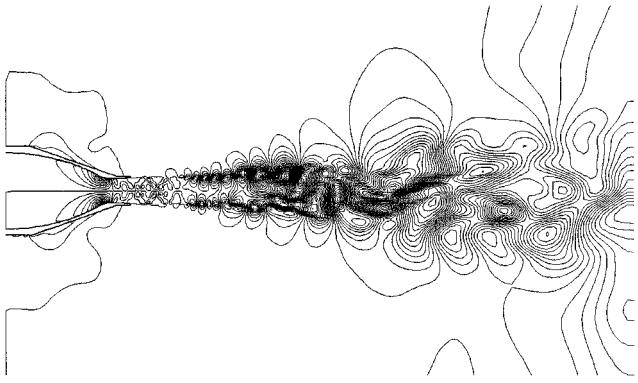

Instantaneous

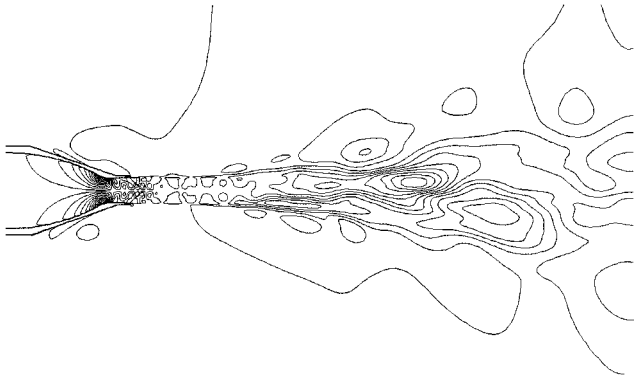

Time averaged

Fig. 3 Radial velocity contours.

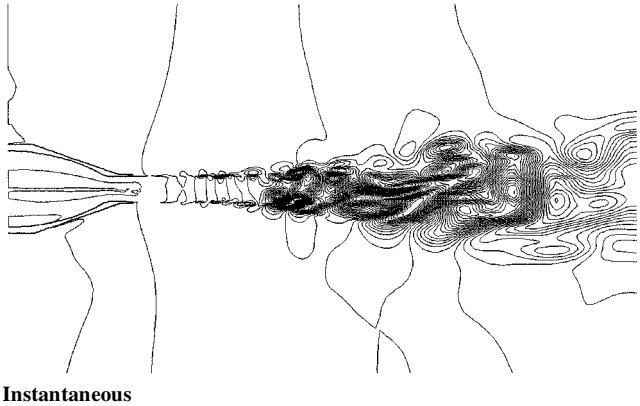

Instantaneous

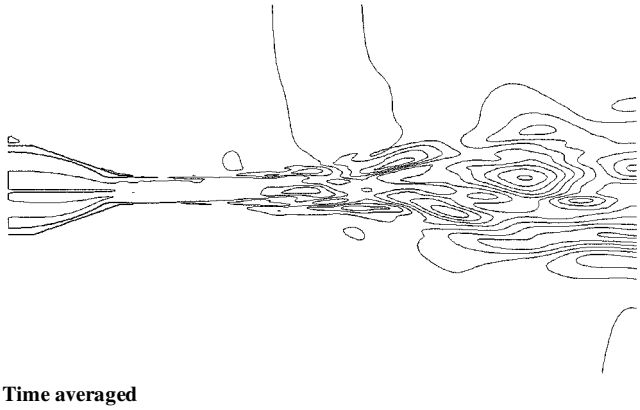

Time averaged

Fig. 4 Azimuthal velocity contours.

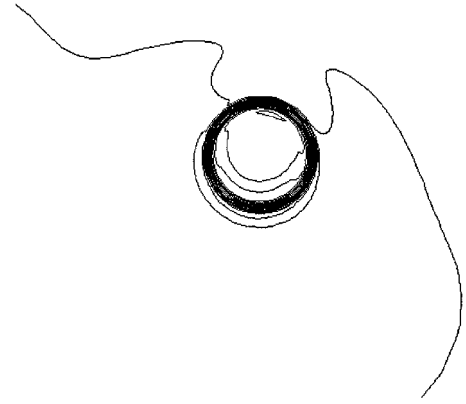

Instantaneous

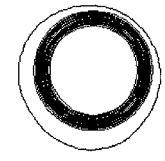

Time averaged

Fig. 5 Total velocity contours at $x/D_j = 3$.

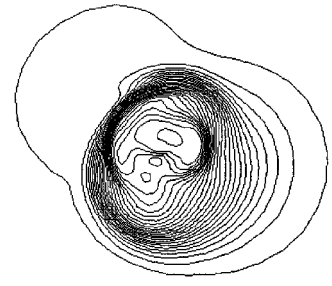

Instantaneous

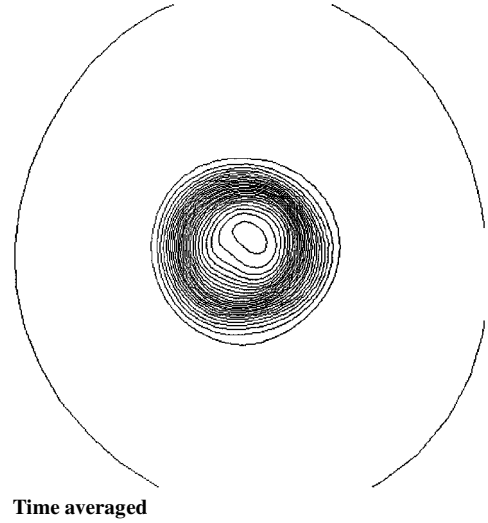

Time averaged

Fig. 6 Total velocity contours at $x/D_j = 6$.

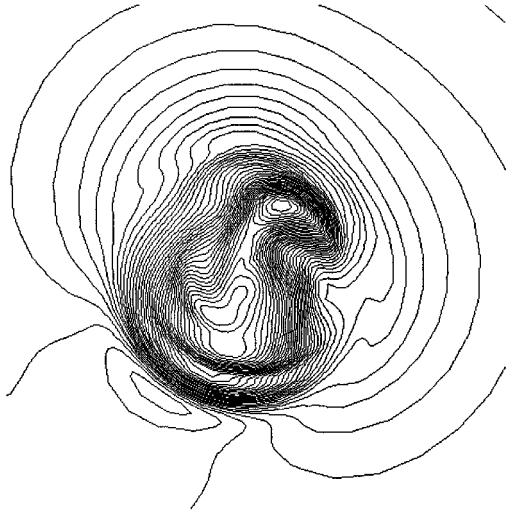

Instantaneous

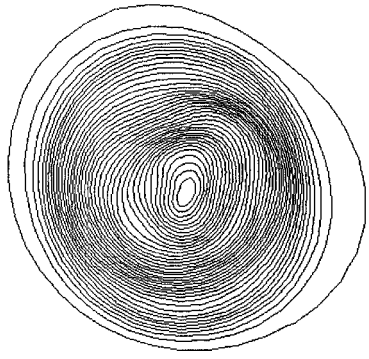

Time averaged

Fig. 7 Total velocity contours at $x/D_j = 9$.

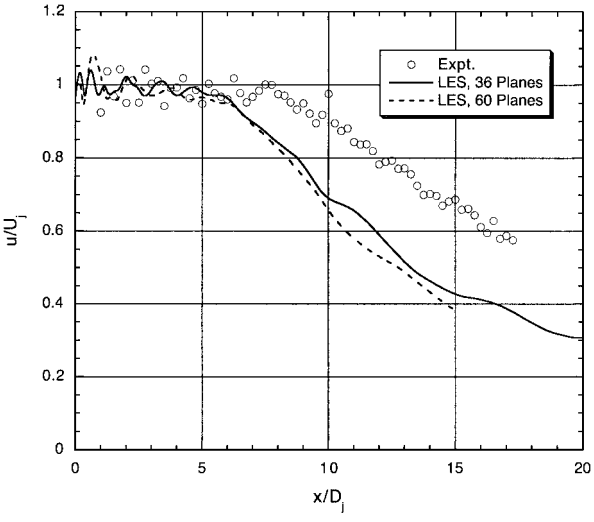

Fig. 8 Time-averaged centerline velocity profile.

Comparison with Experiment

The time-averaged velocity profiles, for both coarse and fine grids, on the jet centerline are compared to experimental data in Fig. 8. Both grids yielded very similar solutions. The fine grid displayed a stronger initial shock and expansion waves near the nozzle exit and a slightly more rapid decay of the centerline velocity beyond the end of the potential core. Both LES solutions predict that the length of the potential core $\mathcal{L}$ is shorter than found experimentally.

Table 2 Error in location of the end of the potential core

Researchers	M_j	Re_j	$\mathcal{L}_{\text{LES}} - \mathcal{L}_{\text{exp}}/D_j$
Present study	1.4	1.2×10^6	−1.5
Gamet and Estivalezes[14]	2.0	2.7×10^6	+5.0
Boersma and Lele[15]	0.9	3.6×10^3	+2.8
Constantinescu and Lele[16]	0.9	3.6×10^3	+3.5

The difference between the LES simulation and the data is about 1.5 jet diameters. This result differs from others in the literature where the length of the potential core is consistently overpredicted. Gamet and Estivalezes[14] simulated a high-Reynolds-number Mach 2 jet, and the LES overpredicted the potential core length by about 5 jet diameters. Boersma and Lele's simulation of a Mach 0.9 jet with a Reynolds number of 3.6×10^3 (Ref. 15) overpredicted the length of the potential core by approximately 2.8 jet diameters. Constantinescu and Lele[16] also simulated a Mach 0.9, 3.6×10^3 Reynolds-number jet. They overpredicted the core length by 3.5 jet diameters and attribute the discrepancy to the "absence of the jet nozzle in simulations, and the shear-layer state (quasi-laminar)." In fact, in all of these past works the nozzle geometry was not modeled. This leads to a poor representation of the initial portion of the jet mixing layer and its development. Table 2 summarizes these comparisons. This study represents a improvement in potential core length prediction of approximately 50% over very low-Reynolds-number simulations, where accuracy would be expected to be better as a result of the direct simulation of larger portion of the turbulent scales. For the high-Reynolds-number case, which is most comparable to the present study, an improvement of 70% is found.

The shorter potential core, in the present simulation, indicates that the turbulent eddies are too energetic, invoking too much mixing. The subgrid model may not be providing adequate dissipation of the large-scale eddies. Adjusting the constants in the Smagorinsky model might improve the predictions. But, a rigorous study to determine the optimal values for these constants is cost prohibitive. The rate of velocity decay beyond the potential core is very close to that of the experimental data. In addition, the shock structure near the nozzle exit is not well resolved in the computation.

Radial profiles of axial velocity at $x/D_j = 2$, 4, 6, 8, 10, and 12 are shown in Fig. 9. Again, the coarse and fine grid predictions are very similar. At $x/D_j = 2$ and 4 the prediction shows less spreading than the experimental data. The fine grid predicts a slightly thicker mixing layer. Because the grid resolution is not sufficient to capture the turbulent structures in this region, the subgrid model should provide the equivalent effect through increased eddy viscosity. The fact that both LES solutions predict less jet spreading than the experiment, with the fine grid solution closer to the experimental data, is a second indication that the subgrid model is not producing adequate dissipation.

Although the agreement with the experimental data is far from perfect, this calculation demonstrates improvement over other high-Reynolds-number LES calculations in the literature. This can be attributed to the complete modeling of the nozzle geometry and the numerical scheme used.

Two-Point Correlations

The statistical characteristics of a turbulent jet have a profound effect on the sound it produces. These characteristics are fundamental to Lighthill's theory of sound generation.[17,18] In this study the integral length scale and convection velocity of the turbulent structures in the mixing layer were characterized using two-point correlations. Chu[19] obtained two-point correlations experimentally for a low-speed jet using hot-wire anemometry. He used these data and a form of Lighthill's equation to compute the jet noise. Scott[20] presented preliminary two-point correlation data, obtained with CFD, for Chu's jet. This study attempts to improve on Scott's analysis, for a high-speed jet, and show that computational techniques can be used to characterize the turbulent structures for application to Lighthill's acoustic analogy.

The general form of the two-point space-time correlation coefficient is

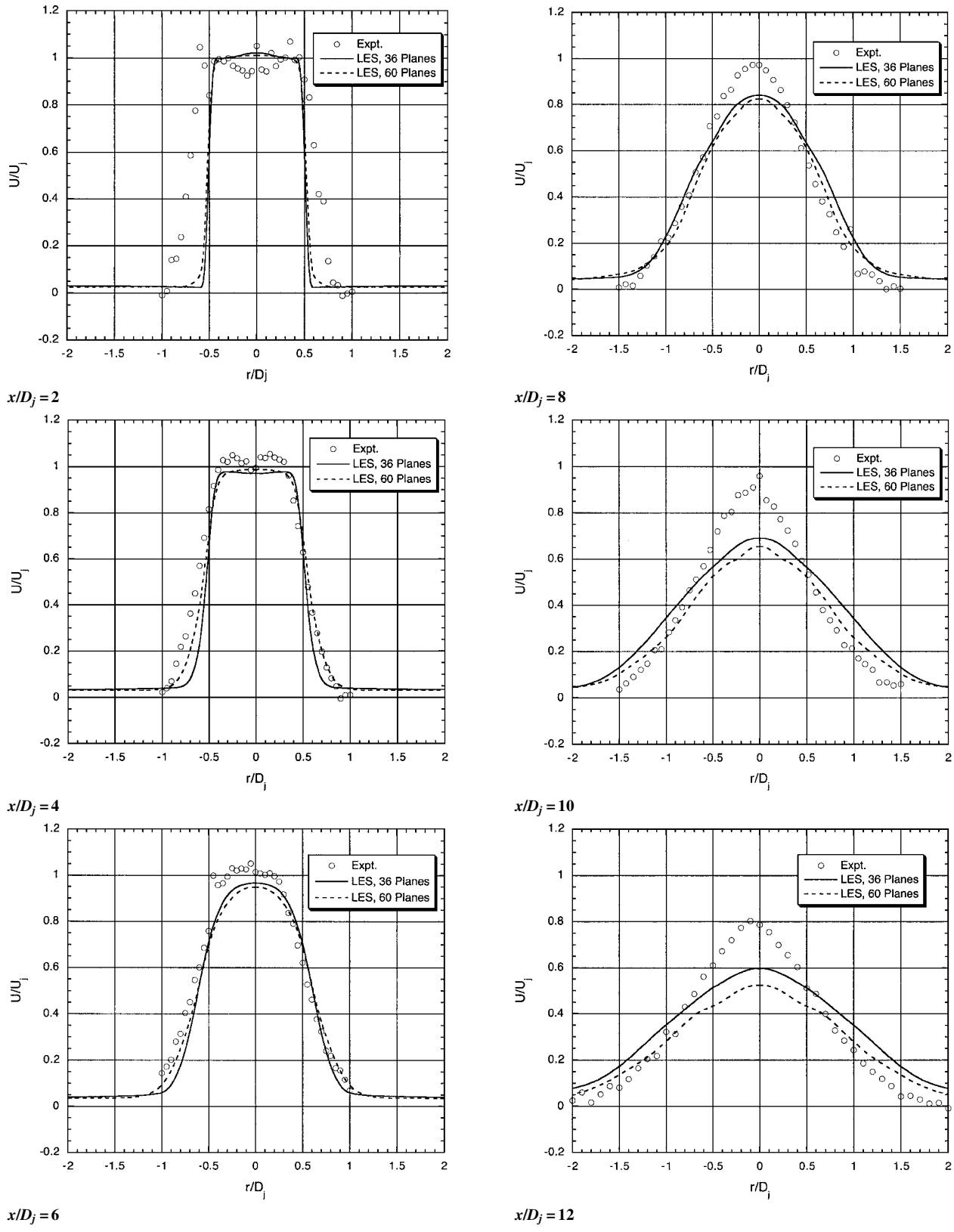

Fig. 9 Time-averaged radial profiles of axial velocity.

$$\mathcal{R}(\psi_i, \tau) = \frac{\overline{\overline{U''_\theta(\phi_i - \psi_i/2, t)U''_\theta(\phi_i + \psi_i/2, t+\tau)}}}{\overline{\overline{U''^2_\theta}}(\phi_i, t)} \tag{12}$$

where the double superscripts $\overline{\overline{()}}$ and $()''$ are used to distinguish time-averaging procedures from the spatial filtering for the LES equations. The position vector ϕ_i and the separation vector ψ_i are shown in Fig. 10. The delay time, the time difference between the upstream and downstream signals, for the space-time correlation is given by τ.

Eight pairs of axial and radial velocity signals with separation distances from $0.125D_j$ to $1.000D_j$ in $0.125D_j$ increments were obtained in the jet mixing layer. The two points where the data were taken were centered about a location six diameters downstream of the nozzle exit on the jet lip line. The two velocity components can be combined to obtain the velocity magnitude in the direction making an angle θ with the jet axis.

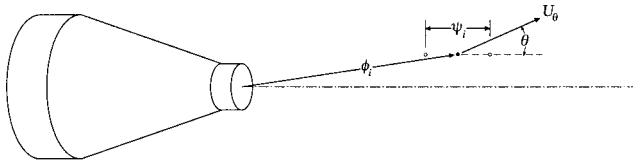

Fig. 10 Schematic for two-point space-time correlations.

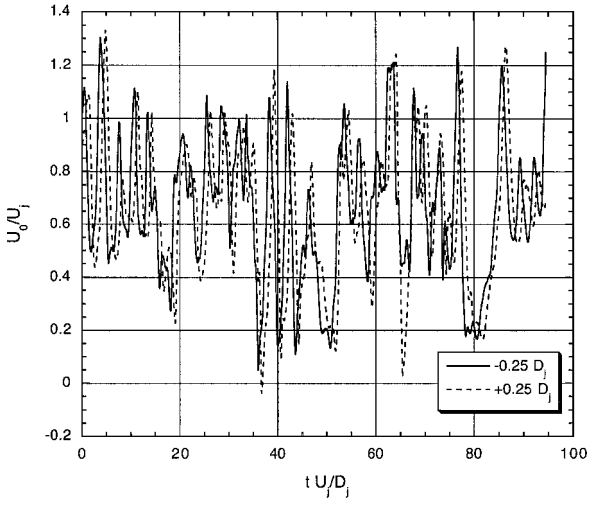

0 deg

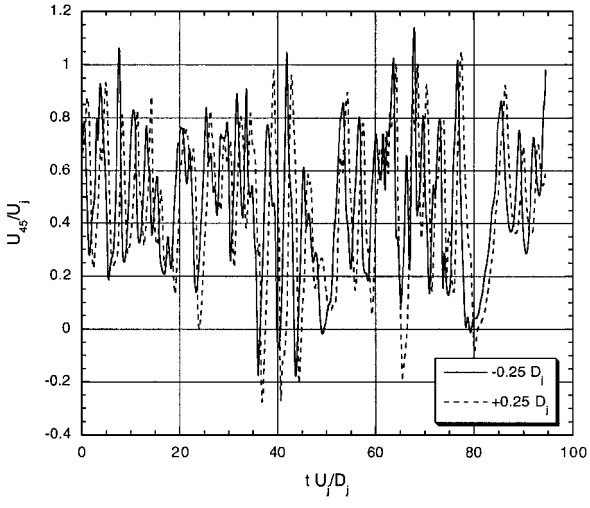

45 deg

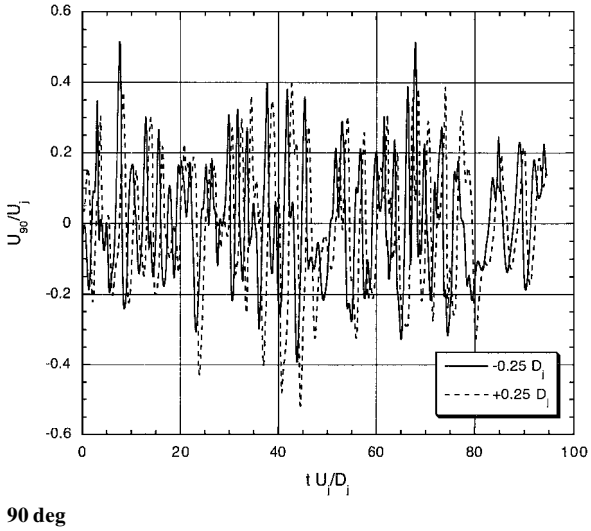

90 deg

Fig. 11 Velocity history for two-point correlations.

Table 3 Velocity statistics at the two-point correlation location

θ	$\bar{\bar{U}}_\theta/U_j$	$\hat{\hat{U}}_\theta/U_j$
0	0.65417	0.26473
45	0.46029	0.26601
90	−0.0032162	0.17076

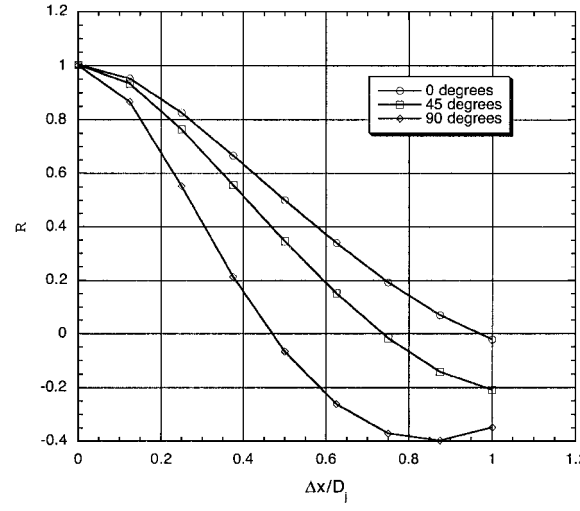

Fig. 12 Two-point space correlation coefficient.

$$U_\theta = u\cos\theta + v\sin\theta \tag{13}$$

Eleven hundred samples, taken at every 100 iterations, were used for the correlations. Time histories of the velocity signals at the points for the fourth separation $\frac{1}{2}\ D_j$ are shown in Fig. 11. Three angles are examined 0, 45, and 90 deg. The average velocity and turbulent intensity for each angle are given in Table 3.

Two-Point Space Correlation

Two-point space correlations can be used to estimate an integral length scale of the flow. The correlations provide a measure of the "similarity" of the velocity signals at two points separated by a fixed distance but at the same instant in time. When the correlation is near unity, one can assume that the velocity signal at both points is caused by the same disturbance or turbulent eddy. By examining two-point correlations at several separation distances, we can obtain a measure of the size of the eddy. A plot of the two-point correlation coefficients vs separation distance is shown in Fig. 12. The correlation of the velocity signal decreases toward zero with increasing separation distance indicating that the average size of the turbulent structures is less than the maximum separation distance (one jet diameter). A rough estimate of the integral length scale was made using the following expression:

$$\ell = \int_0^\infty \mathcal{R}(\psi_i, 0)\,\mathrm{d}\psi_i \tag{14}$$

To evaluate the integral, the data were fitted with a sixth-order polynomial using the method of least squares. The polynomial was then integrated analytically to obtain the length scale. The results are shown in Table 4. The data at 0 deg indicate that the extent of turbulent structures in this direction are approximately $\frac{1}{2}D_j$. The smaller length scales obtained from the 45- and 90-deg data are caused by the relatively large region of negative correlation coefficients for these data. This effect was also noted by Chu.[19]

Two-Point Space-Time Correlations

Two-point space-time correlations can be used to determine the convection velocity of a turbulent eddy. For a given separation distance a series of two-point correlations are computed, where the downstream velocity signal is delayed by an increasing amount of time. The delay time at which the downstream signal is correlated

Table 4 Integral length scales

θ	ℓ/D_j
0	0.50161
45	0.37032
90	0.10422

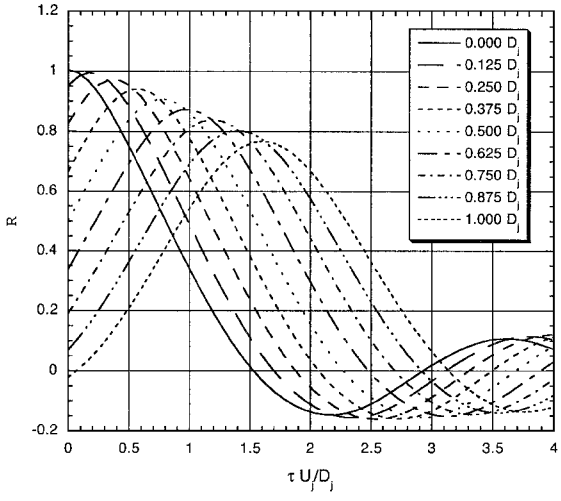

0 deg

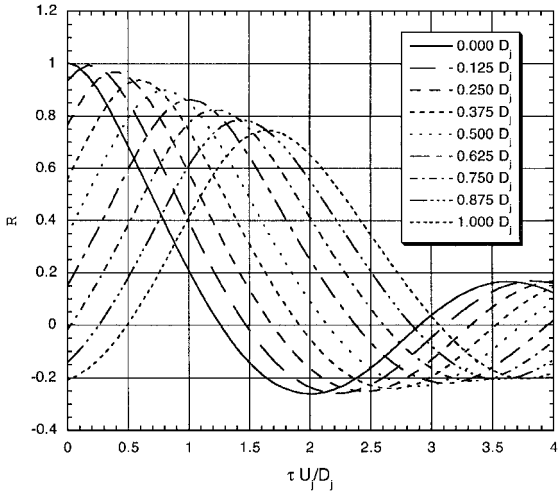

45 deg

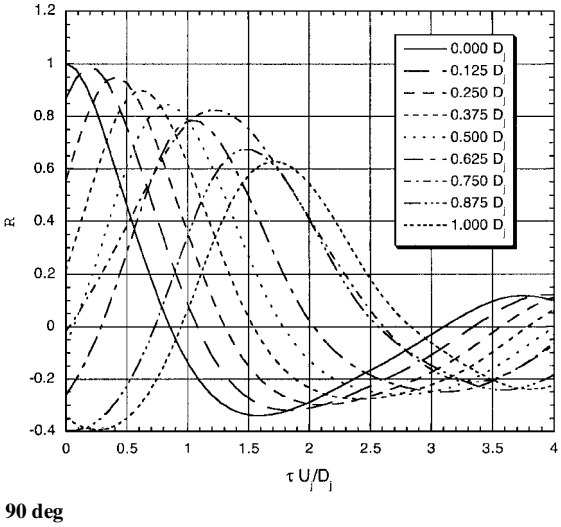

90 deg

Fig. 13 Two-point space-time correlation coefficient.

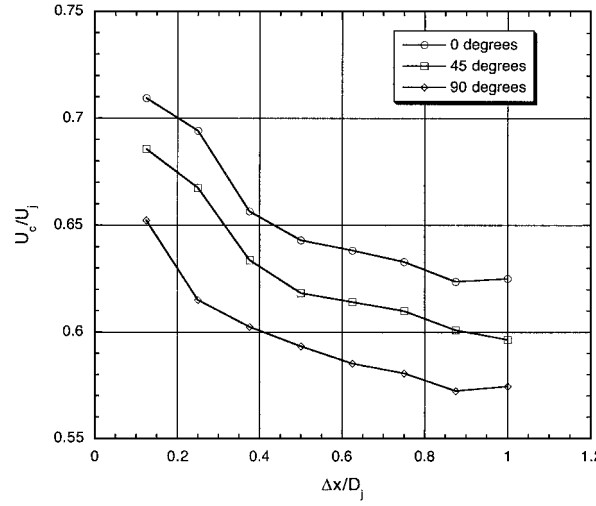

Fig. 14 Convection velocity.

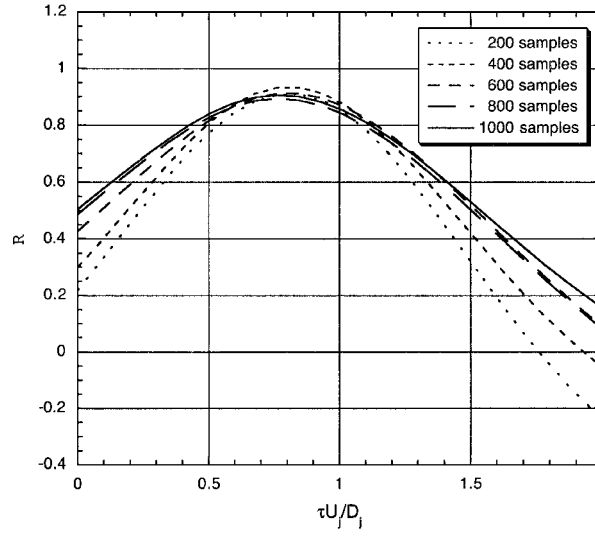

Fig. 15 Convergence of the two-point space-time correlation.

with the upstream signal is the time that was required for the disturbance at the upstream point to convect to the downstream point. The convection speed is simply the ratio of the separation distance to the delay time. Plots of the two-point space-time correlations for each separation are shown in Fig. 13. For each separation there is a delay time where the signals are clearly correlated (a distinct peak in the correlation curve). This delay time increases with increasing separation distance.

The exact location of the maximum correlation coefficient cannot be determined from the discrete data obtained in the analysis. To find this location, the correlation data were again curve fit with a polynomial. The maximum in the curve is found by differentiating the polynomial equation. The resulting convection speed U_c is shown in Fig. 14. The computed convection speeds ranged from 0.57 to 0.71 U_j depending on angle and separation distance. For comparison the convection velocity given by Papamoschou and Roshko[21] was computed:

$$U_{c_{\text{theory}}} = \frac{a_\infty U_j + a_j U_\infty}{a_j + a_\infty} \tag{15}$$

The theoretical velocity 0.56 U_j is lower than the LES derived velocities. As previously noted by Thurow et al.,[22] this result is consistent with the "stream selection rule" of Dimotakis,[23] which says for compressible shear layers with a supersonic and a subsonic stream the convection velocity of the structures will deviate from the theoretical value toward the supersonic value. The convection speed decreases with increasing separation distance as a result of viscous effects.

The effect of the relatively short averaging time on the correlations was explored by studying the convergence of the correlation curve with increasing number of samples. Five sets of two-point space-time correlations at the $\frac{1}{2}D_j$ separation distance were computed using the first 200, 400, 600, 800, and 1000 samples. Figure 15 plots the correlation curves for each sample size in the region of interest (near the peak of the correlation). It is clear that the correlation curve has converged, and that the location of peak in the curve (the quantity of interest) will not change with additional sampling.

Summary

A large-eddy simulation of a turbulent compressible jet was performed. A nearly perfectly expanded axisymmetric jet with an exit Mach number of 1.4 and Reynolds number of 1.2×10^6 was analyzed.

The Favre-filtered Navier–Stokes equations were solved using a uniformly fourth-order-accurate numerical scheme. The scheme is based on a low-dispersion Runge–Kutta time-stepping stepping and uses a fourth-order central difference spatial operator. Artificial dissipation, for stability, is added through solution filtering. Subgrid-scale models are adapted from compressible forms of Smagorinsky's original model. The resulting flow solver was run on a shared memory parallel computer.

The calculations showed that this LES simulation accurately captures the physics of the turbulent jet. The agreement with experimental data relatively is good and improves on results in the current literature. However, there is still much room for improvement. The improved agreement over previous work can be attributed to the new numerical scheme and the modeling of the nozzle lip and its effect on the mixing layer.

A two-point correlation technique was used to quantify the turbulent structures. This work showed that computational methods can be used to statistically characterize the turbulent structures for use in Lighthill's acoustic analogy. Two-point space correlations were used to obtain a measure of the integral length scale, which proved to be approximately $\frac{1}{2}D_j$. Two-point space-time correlations were used to obtain the convection velocity for the turbulent structures. This velocity ranged from 0.57 to 0.71 U_j and is in agreement with the stream selection theory of Dimotakis.[23]

There are two recommendations for further work:

1) Further research into improving the subgrid-scale models is necessary.

2) The time required to run a simulation on this relatively simple geometry severely limits the usefulness of LES. This limit can be eased if a more efficient numerical method is found. As shown, the time-stepping scheme is typically the factor that limits the computational efficiency. A high-order accuracy efficient time-stepping scheme would allow faster turnaround of solutions and more accurate answers on finer grids.

Although there is room for improvement in accuracy, this research has shown that large-eddy simulation can be used, as is, to provide new insight and information about high-Reynolds-number jet flows. The characterization of the turbulent structures, integral length scale and convection velocity, can be used to develop improved tools for predicting the fluid mechanics and acoustics of jets.

References

[1]Panda, J., and Seasholtz, R. G., "Density Fluctuation Measurement in Supersonic Fully Expanded Jets Using Rayleigh Scattering," AIAA Paper 99-1870, May 1999.

[2]Panda, J., and Seasholtz, R. G., "Velocity and Temperature Measurement in Supersonic Free Jets Using Spectrally Resolved Rayleigh Scattering," AIAA Paper 99-0296, Jan. 1999.

[3]Panda, J., and Zaman, K. B. M. Q., "Measurement of Initial Conditions at Nozzle Exit of High Speed Jets," AIAA Paper 2001-2143, May 2001.

[4]Smagorinsky, J., "General Circulation Experiments with the Primitive Equations, Part I: The Basic Experiment," *Monthly Weather Review*, Vol. 91, March 1963, pp. 99–152.

[5]Moin, P., Squires, K., Cabot, W., and Lee, S., "A Dynamic Subgrid-Scale Model for Compressible Turbulence and Scalar Transport," *Physics of Fluids A*, Vol. 3, No. 11, 1991, pp. 2746–2757.

[6]Vreman, B., Geurts, B., and Kuerten, H., "Subgrid-Modelling in LES of Compressible Flows," *Direct and Large-Eddy Simulation I*, edited by P. R. Voke, Kluwer Academic, Norwell, MA, 1994, pp. 133–144.

[7]Erlebacher, G., Hussaini, M. Y., Speziale, C. G., and Zang, T. A., "Toward the Large-Eddy Simulation of Compressible Turbulent Flows," NASA CR 187460, Oct. 1990.

[8]DeBonis, J. R., "The Numerical Analysis of a Turbulent Compressible Jet," Ph.D. Dissertation, Dept. of Aerospace Engineering and Aviation, The Ohio State Univ., Columbus, OH, Dec. 2000.

[9]DeBonis, J. R., and Scott, J. N., "Truncation Error Characteristics of Numerical Schemes for Computational Aeroacoustics," AIAA Paper 2001-1098, May 2001.

[10]Carpenter, M. H., and Kennedy, C. A., "Fourth-Order 2N-Storage Runge-Kutta Schemes," NASA TM 109112, June 1994.

[11]Kennedy, C. A., and Carpenter, M. H., "Comparison of Several Numerical Methods for Simulation of Compressible Shear Layers," NASA TP 3484, Dec. 1997.

[12]Barber, T. J., Chiapetta, L. M., DeBonis, J. R., Georgiadis, N. J., and Yoder, D. A., "Assessment of the Parameters Influencing the Prediction of Shear Layer Mixing," *Journal of Propulsion and Power*, Vol. 15, No. 1, 1998, pp. 45–53.

[13]Boluriaan, S., Morris, P. J., Long, L. N., and Scheidegger, T., "High Speed Jet Noise Simulations for Noncircular Nozzles," AIAA Paper 2001-2272, May 2001.

[14]Gamet, L., and Estivalezes, J. L., "Application of Large-Eddy Simulations and Kirchoff Method to Jet Noise Prediction," *AIAA Journal*, Vol. 36, No. 12, 1998, pp. 2170–2178.

[15]Boersma, B. J., and Lele, S. K., "Large Eddy Simulation of a Mach 0.9 Turbulent Jet," AIAA Paper 99-1874, May 1999.

[16]Constantinescu, G. S., and Lele, S. K., "Large Eddy Simulation of a near Sonic Turbulent Jet and Its Radiated Noise," AIAA Paper 2001-0376, Jan. 2001.

[17]Lighthill, M. J., "On Sound Generated Aerodynamically, I. General Theory," *Proceedings of the Royal Society of London, Series A: Mathematical and Physical Sciences*, Vol. 211, 1952, pp. 564–587.

[18]Lighthill, M. J., "On Sound Generated Aerodynamically, II. Turbulence as a Source of Sound," *Proceedings of the Royal Society of London, Series A: Mathematical and Physical Sciences*, Vol. 222, Feb. 1954, pp. 1–32.

[19]Chu, W. T., "Turbulence Measurements Relevant to Jet Noise," Univ. of Toronto Inst. for Aerospace Studies, Rept. 119, Toronto, ON, Canada, Nov. 1966.

[20]Scott, J. N., "A Comparison of Numerical and Experimental Results for Unsteady Flow Associated with Jet Noise," AIAA Paper 94-0459, Jan. 1994.

[21]Papamoschou, D., and Roshko, A., "The Compressible Turbulent Shear Layer: An Experimental Study," *Journal of Fluid Mechanics*, Vol. 197, Dec. 1988, pp. 453–477.

[22]Thurow, B., Lempert, W., and Samimy, M., "MHZ Rate Imaging of Large-Scale Structures Within a High Speed Axisymmetric Jet," AIAA Paper 2000-0659, Jan. 2000.

[23]Dimotakis, P. E., "On the Convection Velocity of Turbulent Structures in Supersonic Shear Layers," AIAA Paper 91-1724, June 1991.

W. J. Devenport
Associate Editor